IEEE Access
Multidisciplinary | Rapid Review | Open Access Journal

Received 26 October 2022, accepted 10 December 2022, date of publication 14 December 2022, date of current version 28 December 2022.

Digital Object Identifier 10.1109/ACCESS.2022.3229071

RESEARCH ARTICLE

Two-Stage ML Detector Using Absolute Value of IQ Components and SVM for Adaptive OFDM-IM

JEONGBIN SEO, HEETAE JIN, DONGHEE YI, AND SUK CHAN KIM, (Senior Member, IEEE)
Department of Electronics Engineering, Pusan National University, Busan 46241, South Korea

Corresponding author: Suk Chan Kim (sckim@pusan.ac.kr)

This work was supported in part by the Korea Ministry of Land, Infrastructure and Transportation (MOLIT) as Innovative Talent Education Program for Smart City; and in part by the Human Resources Development Program of the Korea Institute of Energy Technology Evaluation and Planning (KETEP) Grant through the Korea Government Ministry of Trade, Industry and Energy, under Grant 20204030200030.

ABSTRACT Among various index modulation technology, adaptive orthogonal frequency division multiplexing with index modulation (A-OFDM-IM) improves reliability by solving the problem of deep fading. However, the maximal likelihood (ML) detector of A-OFDM-IM has high complexity by simultaneously performing active subcarrier detection and quadrature amplitude modulation (QAM) symbol demodulation. A simpler type of ML detector can be applied since the A-OFDM-IM has independent active states of each subcarrier and uses a single QAM constellation. In this paper, we propose two low-complexity detectors for the A-OFDM-IM. The proposed detectors have a two-stage receiving process, active subcarrier detection, and QAM demodulation. In active subcarrier detection, the presence or absence of the QAM symbol is more important than its information. Therefore we derive the thresholds using the absolute value of the in-phase and quadrature components of the received signal in the frequency domain. Using the absolute value, the distribution of noise added to inactive subcarrier is half normal. This is different from noise distribution of the ML detector, and the proposed detectors select the threshold considering the corresponding noise distribution. The first proposed detector uses a threshold derived by the ML estimation method. The second detector estimates the active subcarriers via a support vector machine. The proposed detectors have lower complexity than the ML detector because of the divided receiving process. Moreover, the theoretical analysis and simulation results show that the proposed detectors have better reliability than the ML detector due to different noise distribution and thresholds.

INDEX TERMS Index modulation, support vector machine, low complexity detector, OFDM.

I. INTRODUCTION

In recent years, owing to the demand for high data rate and reliability, there are many researches for promising next-generation modulation technologies. Index modulation (IM) is considered as a potential candidate because of its high spectral efficiency (SE), energy efficiency (EE), and reliability [1]. IM is a modulation technology that delivers information not only through the phase shift keying (PSK)/ quadrature amplitude modulation (QAM) symbols but also through the index of the selected communication resources such as subcarriers, time slots, antennas, and radio frequency mirrors. Among the various IM technologies, orthogonal frequency division multiplexing with index modulation (OFDM-IM) is an application of IM in the frequency domain. OFDM-IM generates a signal by selecting active subcarriers using a combinatorial or look-up table method for input bits and allocating PSK/QAM symbols to the active subcarriers [5]. It has a higher data rate and reliability compared with the conventional OFDM. Since the introduction of OFDM-IM, many studies have been conducted to improve its spectral efficiency and reliability. To improve spectral

The associate editor coordinating the review of this manuscript and approving it for publication was Long Wang.

efficiency, IM technologies that use multiple PSK/QAM constellations while reducing the number of null subcarriers have been proposed. The corresponding IM technologies include dual-mode IM-aided OFDM (DM-OFDM), multiple-mode OFDM-IM (MM-OFDM-IM), layered OFDM-IM (L-OFDM-IM), and super-mode OFDM-IM (SuM-OFDM-IM) [8], [9], [10], [11]. DM-OFDM divides subcarriers into two groups, A and B, and allocates two constellation alphabets, $\mathcal{M}_A$ and $\mathcal{M}_B$. Spectrum resource utilization is increased by using all subcarriers. MM-OFDM-IM uses all subcarriers, similar to DM-OFDM, but it permutes multiple PSK/QAM constellations (modes) and assigns them to subcarriers. L-OFDM-IM selects multiple active subcarrier sets and allocates PSK/QAM symbols with different constellations for each set. SuM-OFDM-IM has higher spectral efficiency and superior reliability than DM-OFDM and MM-OFDM-IM by jointly selecting the mode activation pattern and subcarrier activation pattern. However, a SuM-OFDM-IM receiver requires a higher computational complexity than DM-OFDM and MM-OFDM-IM.

To improve the reliability of OFDM-IM, adaptive active subcarrier selection technologies considering channel state information (CSI) have been proposed. The corresponding modulation technologies include adaptive OFDM-IM (A-OFDM-IM), enhanced Huffman-coded OFDM-IM (EHC-OFDM-IM), and enhanced OFDM with subcarrier number modulation (E-OFDM-SNM) [12], [13], [15]. To avoid deep fading in relay networks, A-OFDM-IM has been proposed. A-OFDM-IM selects active subcarriers from the mapping scheme (MS), a subset of subcarriers with a high signal-to-noise ratio (SNR) of the received signal. By using the MS, A-OFDM-IM reduces the degradation due to deep fading. EHC-OFDM-IM uses Huffman code to select the active subcarriers. Subcarriers with a high channel gain are prioritized by the Huffman code, which improves reliability. E-OFDM-SNM is an improved modulation technology for OFDM-SNM considering the CSI. OFDM-SNM is a modulation technology that transmits information by number rather than indexes of active subcarriers and has a higher SE than OFDM-IM when binary PSK (BPSK) is used [14]. E-OFDM-SNM reduces the effect of attenuation due to deep fading by using a subset of subcarriers with a high channel gain similar to A-OFDM-IM.

The IM detector estimates the active subcarriers and QAM symbols. General IM detectors include a maximal likelihood (ML) detector and a log-likelihood ratio (LLR) detector. The ML detector estimates the active subcarriers and QAM symbols simultaneously. Because the ML detector is a joint detector, it has superior performance; however, it has high complexity. The LLR detector demodulates QAM symbols after estimating the active subcarriers. Because the LLR detector is a component-wise detector, its complexity is low, and its performance is similar to that of the ML detector in the high SNR region [5]. However, if some conditions are met, the optimal performance can be obtained while performing active subcarrier detection and QAM demodulation separately. A corresponding condition is that the active states of each subcarrier are independent, and a single QAM constellation is used. The A-OFDM-IM satisfies these conditions. Due to these conditions, the A-OFDM-IM can use a simple ML detector in which active subcarrier detection and QAM symbol demodulation are separated.

In this paper, we propose two low-complexity detectors that can be applied to A-OFDM-IM. The proposed detector divides the receiving process into index detection, which estimates the active subcarriers, and QAM symbol demodulation. By performing index detection first, the complexity is reduced because the QAM symbol demodulation is performed only on the subcarriers estimated as the active subcarrier. In index detection of OFDM-IM with single QAM constellation, it is important to determine the presence or absence of a QAM symbol rather than the information delivered by the QAM symbol. Therefore, the proposed detectors perform index detection using the absolute value of the in-phase and quadrant (IQ) components of the received signal in the frequency domain. In other words, the constellation of the received signal is folded into the first quadrant. Therefore we call obtaining the absolute value of the IQ components a fold to the first quadrant (R^{++}) (FF) operation. When the constellation is folded, the noise distribution is changed from normal distribution to half-normal distribution. Therefore, we designed the first proposed detector by deriving a threshold for index detection in the corresponding distribution. In addition, by using the hyperplane of the support vector machine (SVM) as a threshold, we perform index detection in the second proposed detector. The main contributions of this paper are summarized below.

- We propose two low-complexity detectors for the A-OFDM-IM. The proposed detectors have lower complexity by performing index detection and QAM demodulation separately. The first detector performs index detection using the threshold derived from ML estimation method, and the second detector performs index detection using SVM. The proposed detectors perform index detection in a different noise distribution from the conventional ML detectors due to the FF operation. Due to the use of FF operation and two separate reception processes, the proposed detectors have lower complexity and better reliability performance.
- We analyzed the complexity of the proposed detectors compared to the conventional ML detector according to the QAM order and the MS size of A-OFDM-IM. In addition, we derived the index detection error probability of the first proposed detector and confirmed that it is superior to the conventional ML detector through Monte Carlo simulation.
- Through MATLAB simulation, we analyzed the bit error rate (BER) performance of the ML detector and the proposed detectors according to SNR and QAM order. As a result, the proposed detectors have better reliability than ML detector. In addition, it was confirmed that the second proposed detector performed better than

the first proposed detector in a specific QAM order and SNR.

The rest of this paper is organized as follows. In Section II, we describe the channel conditions considered in this paper and the A-OFDM-IM transmitter. In Section III, we describe the ML detector for performance comparison and the proposed detectors. In Section IV, we derived the index detection error probability of the FML detector. In Section V, we compare the computational complexities of both the proposed detectors and ML detectors. In Section VI, we analyze the BER performances of the ML detector, FML detector, and SVM-aided detector. Finally, Section VII concludes the paper.

II. SYSTEM MODEL

A. CHANNEL MODEL

We assumed that the channel model is a slow-frequency-selective channel [12]. The channel coherence time is sufficient for the transmitter to receive the CSI that is required to select a MS from the receiver [12]. The channel components of each frequency are independent, and the channel gain follows an exponential distribution with average u. The probability density function (PDF) and cumulative distribution function (CDF) of the channel gain are

$$f(\epsilon) = \exp(-\epsilon/u) \Leftrightarrow F(\epsilon) = 1 - \exp(\epsilon/u), \tag{1}$$

where ϵ $(= \left|h(n')\right|^2, \forall n' \in \mathcal{N}_{Total})$ denotes the channel gain and $\mathcal{N}_{Total} = \{1, 2, \ldots, N_T\}$ denotes a set of all subcarriers.

B. TRANSMITTER

The transmitter of the A-OFDM-IM is shown in Fig. 1. The transmitter generates an A-OFDM-IM signal by selecting active subcarriers in the MS and assigning QAM symbols to them [12]. Using the MS, which is a subset of subcarriers with a high SNR, the A-OFDM-IM can mitigate the attenuation caused by deep fading. Therefore, the A-OFDM-IM transmitter requires the CSI from the receiver. The number of total subcarriers is N_T and the number of subcarriers in the MS is N_S, where $1 \leq N_S \leq N_T$.

To make an A-OFDM-IM symbol, a variable length bit stream, $\mathbf{B}(k) = [\mathbf{b}_S^T(k), \mathbf{b}_M^T(m_1), \mathbf{b}_M^T(m_2), \ldots, \mathbf{b}_M^T(m_{N_A(k)})]$, is required, where $k \in \left\{1, 2, \ldots, 2^{N_S}\right\}$ denotes the index of the subcarrier activation pattern (SAP), and $m_t \in \{1, 2, \ldots, M\}$ denotes the index of the QAM symbol for the tth active subcarrier. The M is the QAM order, and the $N_A(k)$ is the number of active subcarriers when the kth SAP is used. The $\mathbf{b}_S(k)$ is a bit stream for selecting active subcarriers and is the same as the decimal number $k-1$ expressed in a binary number. That is, $\mathbf{b}_s(1) = [0, 0, \ldots, 0]$ and $\mathbf{b}_s(2^{N_S}) = [1, 1, \ldots, 1]$. The $\mathbf{b}_M(m_t)$ is the bit stream for the QAM symbol to be allocated to the tth active subcarrier. In the bit splitter, $\mathbf{b}_S(k)$ and $[\mathbf{b}_M^T(m_1), \mathbf{b}_M^T(m_2), \ldots \mathbf{b}_M^T(m_{N_A(k)})]$ are divided and sent to the index selector and QAM modulator, respectively.

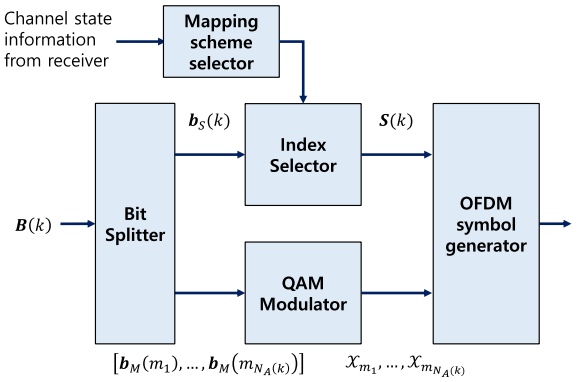

FIGURE 1. A-OFDM-IM transmitter structure.

The index selector determines the active subcarriers in the MS by applying on-off keying (OOK) to $\mathbf{b}_S(k)$. In other words, if the first bit of $\mathbf{b}_S(k)$ is 1, the first subcarrier in the MS is the active subcarrier, and if the bit is 0, the subcarrier is the inactive subcarrier. Therefore, the length of $\mathbf{b}_S(k)$ is N_S. The index selector outputs an activation state matrix, which is

$$\mathbf{S}(k) = \text{diag}\left(b_S(k, 1), b_S(k, 2), \ldots, b_S(k, N_S)\right), \tag{2}$$

where $b_S(k, n)$ denotes the nth entry in $\mathbf{b}_S(k)$, and diag(a, a) denotes a diagonal matrix with diagonal components a, a.

The mapping scheme selector creates a MS using the CSI from the receiver. The formula for selecting the index of MS [12], is

$$\hat{c} = \arg\max_{c \in C} \left\{ \sum_{n \in \mathcal{N}_{MS}(c)} \gamma(2^{N_S}, n) \right\}, \tag{3}$$

where $\hat{c} \in C = \{1, 2, \ldots, {}_{N_T}\mathrm{C}_{N_S}\}$ is an index of the optimal MS and $\gamma(k, n)$ is the SNR of the received signal corresponding to the nth subcarrier in the MS, when the kth SAP is used. The $\mathcal{N}_{MS}(c)$ is a cth MS. If the c is 1, subcarriers from the first to the N_Sth are selected as MS. The received SNR for the nth subcarrier is

$$\gamma(k, n) = \frac{P_T}{N_A(k) N_0} b_S(k, n) \left|h(n)\right|^2, \quad \forall n \in \mathcal{N}_{MS}(c), \tag{4}$$

where P_T is the total transmission power, $|h(n)|^2$ is the channel gain corresponding to the nth subcarrier in the MS, and N_0 is the noise variance.

The Fig. 2 describe an example of process in transmitter of A-OFDM-IM from MS selection to active subcarrier selection for $N_S = 4$. In Fig. 2, a set of subcarriers such as f_1, f_3, f_6, f_8 has higher SNR than other subcarriers. According to (3), mapping scheme selector select a set of the subcarriers as MS. The subcarriers have absolute indices(n') and relative indices(n) respectively. And the index selector selects the subcarriers f_1, f_3, f_6 as active subcarriers due to the $\mathbf{b}_s(k) = 1110_2$.

For $k = 1$, there is no active subcarrier because $\mathbf{b}_S(1)$ is all 0. It is called zero active dilemma [12]. In [12], to solve

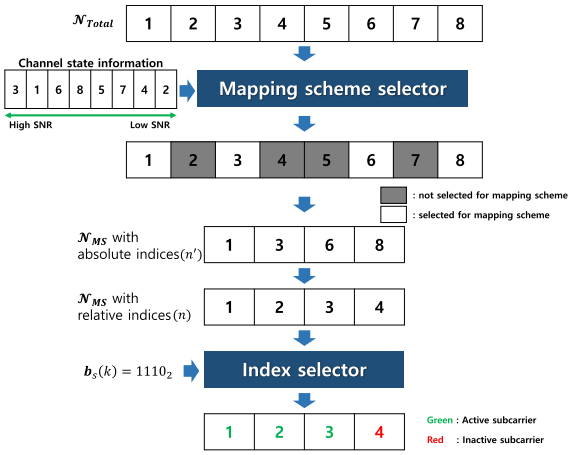

FIGURE 2. Example of process in transmitter of A-OFDM-IM for $N_S = 4$.

the zero active dilemma, a complementary subcarrier ($\tilde{n}$) has been defined.

$$\tilde{n} = \arg \max_{n' \in \mathcal{N}_{Total} \setminus \mathcal{N}_{MS}} \left|h(n')\right|^2. \tag{5}$$

The $\mathcal{N}_{Total}$ denotes a set of total subcarriers. For $k = 1$, one QAM symbol is allocated only to the complementary subcarrier to transmit the input data.

The QAM modulator generates $N_A(k)$ QAM symbols. When the QAM order is M, the QAM symbol to be assigned to the tth active subcarrier is $\mathcal{X}_{m_t} \in \{\mathcal{X}_1, \mathcal{X}_2, \ldots, \mathcal{X}_M\}$.

The OFDM signal generator allocates QAM symbols to active subcarriers, converts them into time-dimension signals using an inverse fast Fourier transform (IFFT), and attaches the cyclic prefix (CP).

When the IFFT size is N_T, the transmitted OFDM signal in the frequency domain is

$$\mathbf{x} = [x(1), x(2), \ldots, x(N_T)]^T \in \mathbb{C}^{N_T \times 1}. \tag{6}$$

For $k \neq 1$, the transmitted signal in the MS is

$$\begin{aligned} &\mathbf{x}(k) \in \mathbb{C}^{N_S \times 1}, \\ &\mathbf{x}(k) = [x(\mathcal{X}_{m_1}, 1), x(\mathcal{X}_{m_2}, 2), \ldots, x(\mathcal{X}_{m_{N_S}}, N_S)]^T, \end{aligned} \tag{7}$$

$$x(\mathcal{X}_{m_n}, n) = \begin{cases} \mathcal{X}_{m_n}, & n \in \mathcal{N}_{AS}(k) \\ 0, & \text{otherwise} \end{cases}, \tag{8}$$

where $\mathcal{N}_{AS}(k)$ is a set of active subcarriers when the kth SAP is used. For $k = 1$, the transmission signal in the frequency domain is

$$x(1) = \mathcal{X}_{m_{\tilde{n}}}, \tag{9}$$

where $\mathcal{X}_{m_{\tilde{n}}}$ is a QAM symbol allocated to the complementary subcarrier($\tilde{n}$).

III. RECEIVER FOR A-OFDM-IM

In subsections A and B, the received signal of the A-OFDM-IM and the conventional ML detector are respectively described. In subsection C, we describe the first proposed detector, the folded maximal likelihood detector. In subsection D, we describe the second proposed detector, the SVM-aided detector.

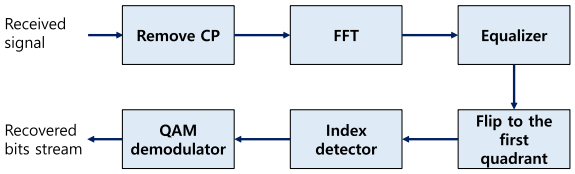

FIGURE 3. Folded maximal likelihood detector structure.

A. RECEIVED SIGNAL

After passing through the channel, for $k \neq 1$, the received A-OFDM-IM signal in frequency domain is

$$\mathbf{y_F}(k) = \sqrt{\frac{P_T}{N_A(k)}} \mathbf{H}_{N_S} \mathbf{x}(k) + \mathbf{w}, \tag{10}$$

$$\mathbf{H}_{N_S} = \text{diag}(h(1), h(2), \ldots, h(N_S)) \in \mathbb{C}^{N_S \times N_S}, \tag{11}$$

where $\mathbf{H}_{N_S}$ is a diagonal matrix consisting of channel components corresponding to the subcarriers in the MS. $\mathbf{w}$ is complex additive white Gaussian noise (AWGN), and each frequency component of $\mathbf{w}$ is independent and identically distributed (iid).

$$\mathbf{w} = [w_1, w_2, \ldots, w_{N_S}]^T \in \mathbb{C}^{N_S \times 1}. \tag{12}$$

For $k = 1$, the received signal is

$$y_F(1) = h(\tilde{n}) \mathcal{X}_{m_{\tilde{n}}} + w(\tilde{n}). \tag{13}$$

B. CONVENTIONAL MAXIMAL LIKELIHOOD DETECTOR

In [12], the ML detector for A-OFDM-IM has been proposed. The ML detector is a joint detector that simultaneously performs index detection and QAM symbol demodulation. The ML detector uses the vector/matrix concatenation operation to demodulate the signal for all SAPs, including for $k = 1$. For arbitrary vectors,

$$\begin{aligned} \mathbf{u}_1 &= [u_1(1), u_1(2), \ldots, u_1(n)]^T \in \mathbb{C}^{n \times 1}, \\ \mathbf{u}_2 &= [u_2(1), u_2(2), \ldots u_2(m)]^T \in \mathbb{C}^{m \times 1}, \end{aligned} \tag{14}$$

the vector concatenation operation is

$$\begin{aligned} &< \mathbf{u}_1, \mathbf{u}_2 > \in \mathbb{C}^{(n+m) \times 1}, \\ &< \mathbf{u}_1, \mathbf{u}_2 > = [u_1(1), \ldots, u_1(n), u_2(1), \ldots u_2(m)]^T, \end{aligned} \tag{15}$$

and for arbitrary diagonal matrices,

$$\begin{aligned} \mathbf{U}_1 &= \text{diag}\,(u_1(1), u_1(2), \ldots, u_1(n)) \in \mathbb{C}^{n \times n}, \\ \mathbf{U}_2 &= \text{diag}\,(u_2(1), u_2(2), \ldots, u_2(m)) \in \mathbb{C}^{m \times m}, \end{aligned} \tag{16}$$

the matrix concatenation operation is

$$\begin{aligned} &< \mathbf{U}_1, \mathbf{U}_2 > \in \mathbb{C}^{(n+m) \times (n+m)}, \\ &< \mathbf{U}_1, \mathbf{U}_2 > = \text{diag}\,(u_1(1), \ldots, u_1(n), u_2(1), \ldots, u_2(m))\,. \end{aligned} \tag{17}$$

To use the ML detector, $\mathbf{X}(k) =< \mathbf{x}(k), \mathcal{X}_{m_{\tilde{n}}} >, \mathbf{H} =< \mathbf{H}_{N_S}, h(\tilde{n}) >$, and $\mathbf{Y}(\mathbf{k}) =< \mathbf{y_F}(k), y_F(1) >$ are defined. The signal demodulated by the ML detector is

$$\hat{\mathbf{X}}(\hat{k}) = \arg\min_{\mathbf{X}(k)} \left\| \mathbf{Y}(k) - \sqrt{\frac{P_T}{N_A(k)}} \mathbf{H}\mathbf{X}(k) \right\|_F, \quad (18)$$

where $\|\cdot\|_F$ denotes the Frobenius norm. The ML detector demodulates the signal by comparing the Euclidean distance (EUD) between the received signal and all candidates for the transmitted signal. Therefore, the EUDs between the inactive subcarrier and QAM symbols must also be calculated, which results in high complexity.

C. FOLDED MAXIMAL LIKELIHOOD DETECTOR

A folded maximal likelihood (FML) detector is described in this subsection. The proposed detector is a components-wise detector that demodulates QAM symbols after index detection. The structure of the FML detector is shown in Fig. 3. After removing the cyclic prefix (CP) of the received signal, FFT is performed to convert the signal to the frequency domain. A one-tap equalizer is used to equalize channel distortion. For index detection, the proposed detector uses absolute values for the each in-phase and quadrature component corresponding to the nth subcarrier of the received signal in the frequency domain,

$$(\mathbf{yI}(k), \mathbf{yQ}(k)) = (|\Re\mathfrak{e}\{\mathbf{y_F}(k)\}|, |\Im\mathfrak{m}\{\mathbf{y_F}(k)\}|), \quad (19)$$

where $\Re\mathfrak{e}\{S\}$ is a function that gets the real part of S, and the $\Im\mathfrak{m}\{S\}$ gets the imaginary part of S. When the absolute value is used, information on a QAM symbol is lost, but the presence or absence of a QAM symbol does not change. Therefore the active subcarriers can be estimated. When the FF operation is performed in the frequency domain, the distribution of the noise added to the inactive subcarrier is changed from a normal distribution to a half-normal distribution. Accordingly a new threshold that is different from the conventional ML detector is required.

The index detection error mainly occurs between the QAM symbol with the lowest power and the origin, which is the case of an inactive subcarrier. In addition, if a threshold is derived by considering the QAM symbol with the lowest power and the origin, other QAM symbols can be determined as active subcarriers because the distance from the threshold is farther than the QAM symbol with the lowest power. Therefore, for simplicity, we derive a new threshold by ML estimation considering the origin and the lowest power symbol. The formula for finding a new threshold is

$$p(y_{(n)}|x_{(n)}(1), h(n)) \gtrless_{H_0}^{H_1} p(y_{(n)}|x_{(n)}(0), h(n)), \quad (20)$$

where $y_{(n)}$ is the output of the FF operation with the nth subcarrier, and $x_{(n)}(0)$ denotes the case where the nth subcarrier is an inactive subcarrier, $x_{(n)}(1)$ denotes the case where the nth subcarrier is an active. H_1 is a hypothesis where the nth subcarrier is an active subcarrier, and H_0 is a hypothesis

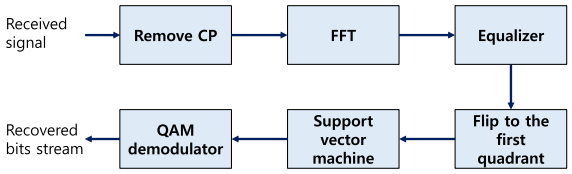

FIGURE 4. Support vector machine-aided detector structure.

where the nth subcarrier is an inactive subcarrier. The new threshold that satisfies (20) is

$$\mathrm{yQ}(k,n) \gtrless_{H_0}^{H_1} -\mathrm{yI}(k,n) + 1 + \ln(4)(\sigma/h(n))^2, \quad (21)$$

where the $\mathrm{yI}(k,n)$ and $\mathrm{yQ}(k,n)$ are the nth components of $\mathbf{yI}(k)$ and $\mathbf{yQ}(k)$, respectively. Please refer to Appendix A for this proof.

The index detector outputs the SAP of the MS with the outputs of FF operation. The QAM demodulator demodulates QAM symbols of the subcarrier corresponding to SAP using ML detection.

D. SVM-AIDED DETECTOR

In order to implement the proposed FML detector, noise variance estimation is required, which is an additional task for conventional communications systems. To avoid noise variance estimation, we propose an SVM-aided detector that performs index detection without noise variance estimation using SVM and FF operation.

In the linear classification problem, the SVM is trained to find the optimal hyperplane, and classifies the data as the hyperplane [23]. The training data of SVM is $(\mathbf{p}_i, q_i)$, where the $\mathbf{p}_i$ is a vector of length L, and the q_i is the label of $\mathbf{p}_i$ and can be $+1$ or -1. The hyperplane of SVM can be expressed by

$$\mathbf{z}^T\mathbf{p}_i - b = 0, \quad (22)$$

where the $\mathbf{z}$ is the normal vector of the hyperplane, and the size is generally 1. The data closest to the hyperplane is called the support vector, and the distance between the hyperplane and the support vector is called the margin. The hyperplanes passing through the support vectors are

$$\begin{aligned} \mathbf{z}^T\mathbf{p}_i - b &= 1, \quad \text{for } q_i = +1, \\ \mathbf{z}^T\mathbf{p}_i - b &= -1, \quad \text{for } q_i = -1. \end{aligned} \quad (23)$$

For all support vectors, the hyperplanes passing through the support vectors can be expressed as

$$q_i\left(\mathbf{z}^T\mathbf{p}_i - b\right) = 1. \quad (24)$$

The distance between the two hyperplanes is $2/\|\mathbf{z}\|$. In order to find the optimal hyperplane, the $2/\|\mathbf{z}\|$ must be maximized, and the problem is the same as minimizing $\|\mathbf{z}\|^2$.

However, if the data cannot be linearly distinguished, the above method cannot be used. To solve this problem, the SVM using kernel function has been proposed [23]. The kernel function $(k(\mathbf{p}, \mathbf{p}_i) = \varphi\{\mathbf{p}\} \cdot \varphi\{\mathbf{p}_i\})$ converts the data into

high-dimensional data that can be linearly distinguished and then performs dot products. Typical kernel functions include linear, polynomial, Gaussian, and hyperbolic tangent function. When the kernel function is used, the hyperplane is

$$\mathbf{z}^T \varphi\{\mathbf{p}_i\} - b = 0. \tag{25}$$

If part of the data is very close to other types of data, it may be impossible to distinguish linearly even if the kernel function is used. To solve this, the hinge loss function is used,

$$\max\left(0, 1 - q_i\left(\mathbf{z}^T \varphi\{\mathbf{p}_i\} - b\right)\right). \tag{26}$$

When the value of the hinge loss function is positive, it means the data exists in the margin of the other side. Therefore, the hinge loss function and $\|\mathbf{z}\|^2$ must be minimized in the form below,

$$\frac{1}{\hat{n}} \sum_{i=1}^{\hat{n}} \max\left(0, 1 - q_i\left(\mathbf{z}^T \varphi\{\mathbf{p}\} - b\right)\right) + \lambda \|z\|^2, \tag{27}$$

where the $\hat{n}$ is the number of training data and the λ is a trade-off parameter between increasing the size of the margin and increasing the number of data located at the margin in the correct direction. The above minimization problem can be rewrote by using a new variable $\beta_i = \max\left(0, 1 - q_i\left(\mathbf{z}^T \varphi\{\mathbf{p}\} - b\right)\right)$.

$$\begin{aligned} &\underset{\mathbf{z},b,\zeta}{\text{minimize}}\, \lambda\|\mathbf{z}\|^2 + \frac{1}{\hat{n}} \sum_{i=1}^{\hat{n}} \beta_i \\ &\text{subject to } q_i\left(\mathbf{z}^T \varphi\{\mathbf{p}_i\} - b\right) \geq 1 - \beta_i \\ &\qquad \beta_i \geq 0\ , \ \text{for } \forall\ i. \end{aligned} \tag{28}$$

The Lagrangian dual problem of this prime problem, [24], is

$$\begin{aligned} &\text{maximize} \sum_{i=1}^{\hat{n}} v_i - \frac{1}{2} \sum_{i=1}^{\hat{n}} \sum_{j=1}^{\hat{n}} q_i q_j v_i v_j k\left(\mathbf{p}_i, \mathbf{p}_j\right) \\ &\text{subject to } \sum_{i=1}^{\hat{n}} v_i q_i = 0 \\ &\qquad 0 \leq v_i \leq \frac{1}{2\hat{n}\lambda},\ \text{for } \forall\ i. \end{aligned} \tag{29}$$

Since the above dual problem is a quadratic problem for v_i, the solution can be found with the quadratic programming algorithm, and the solution is

$$\mathbf{z} = \sum_{i=1}^{\hat{n}} v_i q_i \varphi\{\mathbf{p}_i\}. \tag{30}$$

Therefore the hyperplane is a linear combination of the support vectors. In addition, the bias (b) is $\mathbf{z}^T \varphi\{\mathbf{p}\} - y_i$ due to $q_i\{\mathbf{z}^T \varphi\{\mathbf{p}\} - b\} = 1$.

The structure of the SVM-aided detector is shown in Fig. 4. The proposed detector removes the CP from the received signal, performs the FFT to that signal, equalizes it with one-tap equalizer and performs FF operation. The SVM used in SVM-aided detector performs index detection like index detector in the FML detector. That is, the SVM uses each element of the FF operation output (yI(k, n), yQ(k, n)) as the input. If the nth subcarrier is an active subcarrier, the output of the SVM is $+1$, and if it is an inactive subcarrier, the output is -1. In training the SVM, all QAM symbols, not just the one with the lowest power, are used. Accordingly two proposed detector have different performance in some QAM order. This is confirmed in section VI. As the kernel function of SVM, the simplest linear kernel and Gaussian kernel are used. Because the trained SVM uses an equalized received signal as an input and is trained over a wide range of SNR values, additional learning and noise variance estimation are not required even if the channel changes. If all subcarriers of the MS are inactive, the QAM demodulator demodulates the QAM symbol of the complementary subcarrier ($\tilde{n}$), and otherwise, the QAM symbols of the active subcarrier are estimated by ML detection.

IV. ANALYTICAL INDEX DETECTION ERROR PROBABILITY

In this section, we analytically derive the index detection error probability (IDEP) of the FML detector. When the nth channel coefficient is denoted by $h(n)$, the conditional index detection error probability of the FML detector is given as:

$$\begin{aligned} &p(e|h(n)) \\ &= \frac{1}{2}\left\{P(x_n(0) \to x_n(1)|h(n)) + P(x_n(1) \to x_n(0)|h(n))\right\} \\ &= \frac{1}{2}\int_0^{\infty}\int_{-y'+\alpha}^{\infty} \frac{2}{\pi\sigma^2} e^{-\frac{(x'/h(n))^2+(y'/h(n))^2}{2\sigma^2}}\, dx'\, dy' \\ &\quad + \frac{1}{2}\Big\{\int_0^{\alpha}\int_0^{-y'+\alpha} \frac{1}{2\pi\sigma^2} e^{-\frac{(x'/h(n)-1)^2+(y'/h(n)-1)^2}{2\sigma^2}}\, dx'\, dy' \\ &\quad + \int_0^{\alpha}\int_0^{y'-\alpha} \frac{1}{2\pi\sigma^2} e^{-\frac{(x'/h(n)-1)^2+(y'/h(n)-1)^2}{2\sigma^2}}\, dx'\, dy' \\ &\quad + \int_{-\alpha}^{0}\int_0^{-y'-\alpha} \frac{1}{2\pi\sigma^2} e^{-\frac{(x'/h(n)-1)^2+(y'/h(n)-1)^2}{2\sigma^2}}\, dx'\, dy' \\ &\quad + \int_{-\alpha}^{0}\int_0^{y'-\alpha} \frac{1}{2\pi\sigma^2} e^{-\frac{(x'/h(n)-1)^2+(y'/h(n)-1)^2}{2\sigma^2}}\, dx'\, dy'\Big\}, \end{aligned} \tag{31}$$

where α is $1 + ln(4)(\frac{\sigma}{h(n)})^2$, x' is $yI(k, n)$, y' is $yQ(k, n)$, and $P(a_1 \to a_2)$ is a probability of estimating a_1 as a_2. To obtain the unconditional index detection error probability, the PDF of the nth smallest channel gain among N_T channels is required. To define the PDF, we order the subcarriers according to the channel gain($G(n) = |h(n)|^2$), such as

$$G_{<1>}(\zeta_1) < G_{<2>}(\zeta_2) < \ldots < G_{<N_T>}(\zeta_{N_T}), \tag{32}$$

where ζ_j denotes the index of the subcarrier with the jth smallest channel gain. According to order statistics [26], the PDF of the nth smallest channel gain among the N_T channels is

$$\phi_{<n>}(\epsilon) = \frac{N_T!(F(\epsilon))^{n-1}(1 - F(\epsilon))^{N_T-n} f(\epsilon)}{(n-1)!(N_T - n)!}. \tag{33}$$

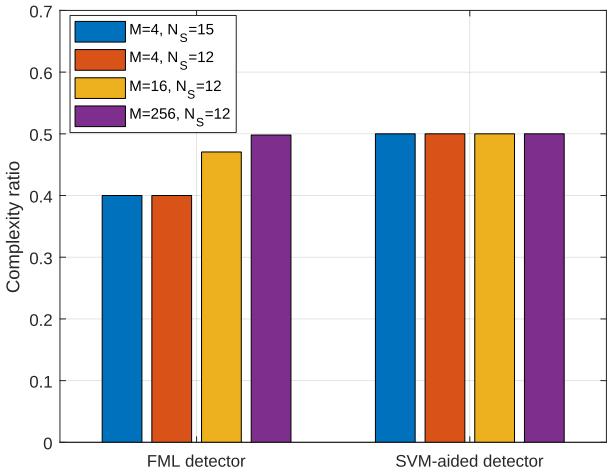

FIGURE 5. Complexity ratio based on ML detector.

TABLE 1. Complexity analysis.

	complexity
ML detector	$4N_S(M+1)$
FML detector	$2N_S M$
SVM-aided detector	$2N_S(1+M)$

Therefore, unconditional IDEP (34), as shown at the bottom of the page. In section VI, we confirm that the IDEP of the FML detector is superior to that of the ML detector through monte-carlo simulation.

V. COMPLEXITY COMPARISON

In this section, the complexities of the ML detector, FML detector, and SVM-aided detector are compared. The complexities of each detector are compared by the number of multiplication operations because the complexity of multiplication is higher than that of other operations [25]. Table 1 shows the complexity of each detector. Fig. 5 shows the complexity ratio of the proposed detectors based on the ML detector in some cases such as $\{M, N_S\} = \{4, 15\}, \{4, 12\}, \{16, 12\}, \{256, 12\}$. The complexity ratios are calculated by dividing the complexities of the proposed detectors by the complexity of the ML detector in each case. In all cases, the proposed detectors have a reduced complexity by more than 50%. We assume that the number of estimated active subcarriers is half of the MS size, which is the average value. For the SVM-aided detector, we calculated the complexity when using a linear kernel. This is because the BER performances are almost the same when using the linear kernel and the Gaussian kernel, as detailed in section VI.

VI. SIMULATION RESULT

In this section, the performances of the ML detector, FML detector, and SVM-aided detector for A-OFDM-IM

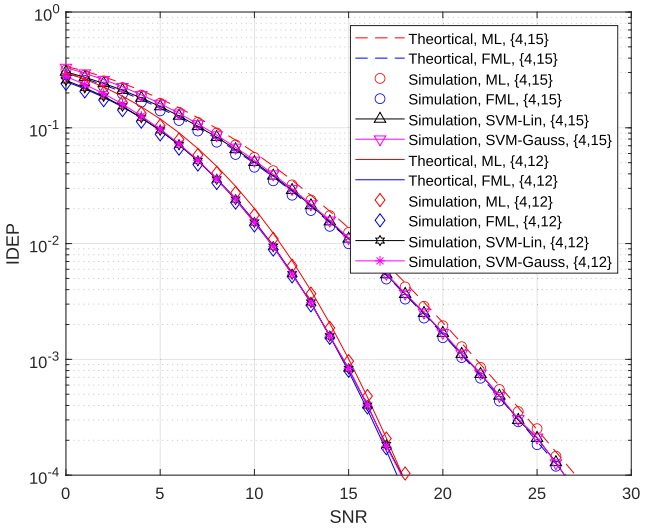

FIGURE 6. IDEP comparison for $M = 4$, $N_S = 12$ and 15.

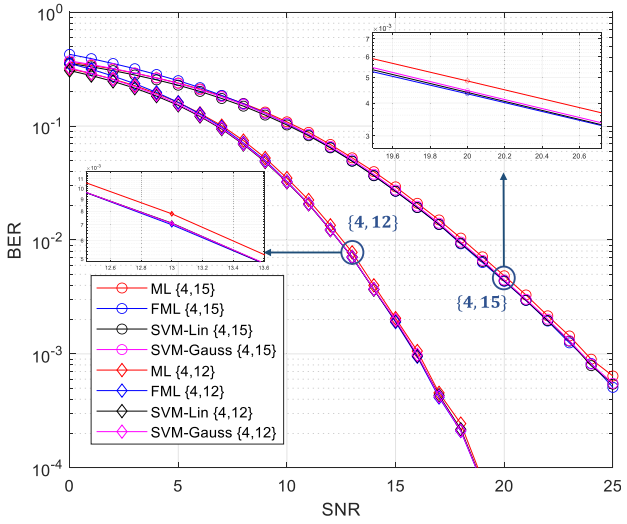

FIGURE 7. BER comparison for $M = 4$, $N_S = 12$ and 15.

are compared. The simulations have been conducted in MATLAB. In all of the simulations, 200,000 A-OFDM-IM signals are transmitted for each SNR. Rayleigh fading is used for the channel, and a perfect CSI is assumed. The SNR denotes E_S/N_0. The total number of subcarriers (N_T) is 16. When training the SVM, 100,000 training data are used for each case. Table 2 shows the SNR range of the SVM training data which are heuristically obtained and the SNR of each training data is uniformly distributed.

Fig. 6 shows the IDEP of the ML detector and the FML detector with the cases $\{M, N_S\} = \{4, 15\}, \{4, 12\}$. In all

$$p(e) = E_h\{p(e|h)\} = \int_0^\infty \int_0^\infty \cdots \int_0^\infty p(e|h) \left(\prod_{n \in \mathcal{N}_S} \phi_{<n>}(G_{<n>}(\zeta_n)) \right) dG_1\, dG_2 \ldots dG_{N_s}. \quad (34)$$

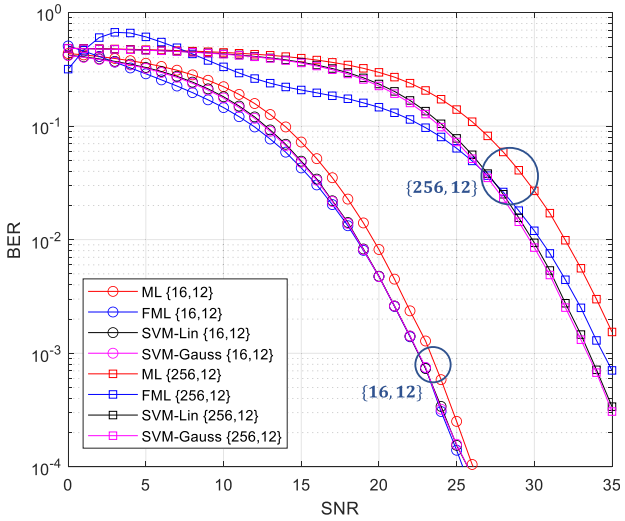

FIGURE 8. BER comparison for $M = 16$ and 256, $N_S = 12$ and 15.

TABLE 2. SNR range of training data.

QAM order(M)	SNR range (dB)
4	(15,25)
16	(20,35)
64	(35,55)
256	(35,55)

cases, the simulation results are almost matched to the analysis results. In most SNR regions, the IDEP of the FML detector is superior to the ML detector. Both the ML detector and the FML detector use the ML estimation method, but there is a performance difference due to different distributions of noise. For the ML detector, all noise is normally distributed. However, in the case of the FML detector, since the FF operation is used, the distribution of noise added to the inactive subcarrier is a half-normal distribution. In other words, the noise environments in which the two detectors perform index detection are different. Both the theoretical analysis and simulation results show that the noise environment of the FML detector is better for index detection.

Fig. 7 shows the BER performances of the proposed detectors and ML detector for the case $\{M, N_S\} = \{4, 15\}, \{4, 12\}$. The SVM-Lin denotes the SVM-aided detector using the linear kernel and the SVM-Gauss denotes the use of the Gaussian kernel. The FML detector and SVM-aided detector have superior BER performance than the ML detector in all SNR regions. In the case of $M = 4$, the performances of the FML detector and SVM-aided detector are similar, since only one QAM symbol exists in the first quadrant when the FF operation is performed. Moreover, in the case of $M = 4$, if the size of MS becomes small, the BER curve becomes round. This is because A-OFDM-IM preferentially selects subcarriers with high SNR when selecting subcarriers to be included in the MS. Therefore, when the small size of the MS is used, subcarriers with severe fading distortion are excluded, and the BER curve is rounded.

Fig. 8 shows the BER performances of the proposed detectors and ML detector for the case $\{M, N_S\} = \{16, 12\}, \{256, 12\}$. In the case of $M = 16$, the BER performances of FML detector and SVM-aided detector are almost same in high SNR region, but in the case of $M = 256$, the SVM-aided detector has a superior BER performance. This is because of the threshold derivation method of the SVM-aided detector. The hyperplane that serves as the threshold of the SVM is determined by the distribution of the support vectors, which are samples close to the other classes [23]. The support vector distribution of the SVM used in the SVM-aided detector depends on the M. When the M is low like 4QAM or 16QAM and the FF operation is performed, one or four QAM symbols exist in the first quadrant. In this case, the support vectors are the samples close to the origin among the samples near the lowest power QAM symbol. However, in case of $M = 256$, if FF operation is performed, 64 QAM symbols exist in the first quadrant, and the samples are relatively widely distributed. Accordingly, the support vector includes samples that are slightly farther away from the origin compared to low M cases. As a result, the hyperplane moves slightly farther away from the origin. As the hyperplane moves away from the origin, the correct detection rate of the inactive subcarrier improves, but the correct detection rate of the active subcarrier with the lowest power QAM symbol decreases. In addition, in the case of $M = 256$, the frequency of occurrence of an inactive subcarrier is 64 times that of an active subcarrier with the lowest power QAM symbol. Therefore, the BER performance of the SVM-aided detector with a better inactive subcarrier estimation performance is superior to the FML detector.

In the case of the SVM-aided detector, the performances of the linear kernel and Gaussian kernel are almost same. This is because the active and inactive subcarrier can be linearly classified. However, the two kernel functions considerably differ in complexity. The complexity of the Gaussian kernel increases proportionally to the number of support vectors. Since our trained SVM has the absolute value of the IQ components of the received signal in the frequency domain as input data, there are many support vectors due to the sporadic distribution of noise. Therefore, the complexity of SVM using Gaussian kernel is high. However, the linear kernel is the least complex kernel function. Therefore, it is more effective to use a linear kernel, because it can achieve a performance that is similar to the Gaussian kernel with lower complexity.

VII. CONCLUSION

In this paper, we have proposed the FML detector and the SVM-aided detector for the A-OFDM-IM. The proposed detectors can be used for A-OFDM-IM which has independent active states of each subcarrier and uses single QAM constellation. In both proposed detectors, we use the FF operation for index detection. The FML detector uses a threshold that is derived by the ML method considering the distribution of the noise added to the inactive subcarrier and the QAM symbol with the lowest power. The SVM-aided

$$\frac{2}{(\sigma/h(n))^2\pi}e^{-\frac{\mathrm{yI}(k,n)^2+\mathrm{yQ}(k,n)^2}{2(\sigma/h(n))^2}} \underset{H_1}{\overset{H_0}{\gtrless}} \frac{1}{2(\sigma/h(n))^2\pi}e^{-\frac{(\mathrm{yI}(k,n)-1)^2+(\mathrm{yQ}(k,n)-1)^2}{2(\sigma/h(n))^2}} \tag{35}$$

$$\ln 4 - \frac{\mathrm{yI}(k,n)^2+\mathrm{yQ}(k,n)^2}{2(\sigma/h(n))^2} \underset{H_1}{\overset{H_0}{\gtrless}} -\frac{(\mathrm{yI}(k,n)-1)^2+(\mathrm{yQ}(k,n)-1)^2}{2(\sigma/h(n))^2} \tag{36}$$

$$\mathrm{yQ}(k,n) \underset{H_0}{\overset{H_1}{\gtrless}} -\mathrm{yI}(k,n)+1+\ln(4)(\sigma/h(n))^2 \tag{37}$$

detector estimates the active subcarriers using the FF operation and SVM. Since the proposed two detectors demodulate the QAM symbols after estimating the active subcarriers, the QAM symbol demodulation is not performed for the inactive subcarrier. Therefore, they have lower complexity than the ML detector. We analyze the active subcarrier estimation performance and BER performances of the FML detector, SVM-aided detector and ML detector. The result indicated that the proposed detectors have superior BER performances than conventional ML detector.

APPENDIX

When the FF operation is performed on the inactive subcarrier, the noise distribution changes from the normal distribution to the half-normal distribution. If v is normal distributed variable with zero mean and σ^2 variance, after FF operation, the PDF of the half normal distribution is

$$f(|v|) = \frac{\sqrt{2}}{\sigma\sqrt{\pi}}e^{-\frac{|v|^2}{2\sigma^2}}. \tag{38}$$

In addition, we assume that the QAM symbol with the lowest power is $1+1i$. The (20) is same with (35), as shown at the top of the page. The left is the PDF of the noise added to the inactive subcarrier, and the right is the PDF of the noise added to the lowest-power QAM symbol. Although the distribution of noise added to the QAM symbol is partially changed, the normal distribution is used as it is. The closed form solution of (26) is (28) which is same with (21).

REFERENCES

[1] S. Sugiura, T. Ishihara, and M. Nakao, "State-of-the-art design of index modulation in the space, time, and frequency domains: Benefits and fundamental limitations," *IEEE Access*, vol. 5, pp. 21774–21790, 2017.
[2] T. Mao, Q. Wang, Z. Wang, and S. Chen, "Novel index modulation techniques: A survey," *IEEE Commun. Surveys Tuts.*, vol. 21, no. 1, pp. 315–348, 1st Quart., 2019.
[3] T. Datta, H. S. Eshwaraiah, and A. Chockalingam, "Generalized space-and-frequency index modulation," *IEEE Trans. Veh. Technol.*, vol. 65, no. 7, pp. 4911–4924, Jul. 2016.
[4] M. I. Kadir, "Generalized space-time-frequency index modulation," *IEEE Commun. Lett.*, vol. 23, no. 2, pp. 250–253, Feb. 2019.
[5] E. Başar, U. Aygölü, E. Panayırcı, and H. V. Poor, "Orthogonal frequency division multiplexing with index modulation," *IEEE Trans. Signal Process.*, vol. 61, no. 22, pp. 5536–5549, Nov. 2013.
[6] R. Fan, Y. J. Yu, and Y. L. Guan, "Generalization of orthogonal frequency division multiplexing with index modulation," *IEEE Trans. Wireless Commun.*, vol. 14, no. 10, pp. 5350–5359, Oct. 2015.
[7] E. Başar, "Multiple-input multiple-output OFDM with index modulation," *IEEE Signal Process. Lett.*, vol. 22, no. 12, pp. 2259–2263, Dec. 2015.
[8] T. Mao, Z. Wang, Q. Wang, S. Chen, and L. Hanzo, "Dual-mode index modulation aided OFDM," *IEEE Access*, vol. 5, pp. 50–60, 2017.
[9] M. Wen, E. Basar, Q. Li, B. Zheng, and M. Zhang, "Multiple-mode orthogonal frequency division multiplexing with index modulation," *IEEE Trans. Commun.*, vol. 65, no. 9, pp. 3892–3906, Sep. 2017.
[10] J. Li, S. Dang, M. Wen, X.-Q. Jiang, Y. Peng, and H. Hai, "Layered orthogonal frequency division multiplexing with index modulation," *IEEE Syst. J.*, vol. 13, no. 4, pp. 3793–3802, Dec. 2019.
[11] A. T. Dogukan and E. Basar, "Super-mode OFDM with index modulation," *IEEE Trans. Wireless Commun.*, vol. 19, no. 11, pp. 7353–7362, Nov. 2020.
[12] S. Dang, J. P. Coon, and G. Chen, "Adaptive OFDM with index modulation for two-hop relay-assisted networks," *IEEE Trans. Wireless Commun.*, vol. 17, no. 3, pp. 1923–1936, Mar. 2018.
[13] S. Dang, S. Guo, J. P. Coon, B. Shihada, and M.-S. Alouini, "Enhanced Huffman coded OFDM with index modulation," *IEEE Trans. Wireless Commun.*, vol. 19, no. 4, pp. 2489–2503, Apr. 2020.
[14] A. M. Jaradat, J. M. Hamamreh, and H. Arslan, "OFDM with subcarrier number modulation," *IEEE Wireless Commun. Lett.*, vol. 7, no. 6, pp. 914–917, Dec. 2018.
[15] S. Dang, G. Ma, B. Shihada, and M.-S. Alouini, "Enhanced orthogonal frequency-division multiplexing with subcarrier number modulation," *IEEE Internet Things J.*, vol. 6, no. 5, pp. 7907–7920, Oct. 2019.
[16] M. Nakao, T. Ishihara, and S. Sugiura, "Dual-mode time-domain index modulation for Nyquist-criterion and faster-than-Nyquist single-carrier transmissions," *IEEE Access*, vol. 5, pp. 27659–27667, 2017.
[17] M. Chen, U. Challita, W. Saad, C. Yin, and M. Debbah, "Artificial neural networks-based machine learning for wireless networks: A tutorial," *IEEE Commun. Surveys Tuts.*, vol. 21, no. 4, pp. 3039–3071, 4th Quart., 2019.
[18] F. Hussain, S. A. Hassan, R. Hussain, and E. Hossain, "Machine learning for resource management in cellular and IoT networks: Potentials, current solutions, and open challenges," *IEEE Commun. Surveys Tuts.*, vol. 22, no. 2, pp. 1251–1275, 2nd Quart., 2020.
[19] C. Zhang, P. Patras, and H. Haddadi, "Deep learning in mobile and wireless networking: A survey," *IEEE Commun. Surveys Tuts.*, vol. 21, no. 3, pp. 2224–2287, 3rd Quart., 2019.
[20] J. W.-H. Kao, S. M. Berber, and V. Kecman, "Blind multiuser detector for chaos-based CDMA using support vector machine," *IEEE Trans. Neural Netw.*, vol. 21, no. 8, pp. 1221–1231, Aug. 2010.
[21] K. M. Thilina, K. W. Choi, N. Saquib, and E. Hossain, "Machine learning techniques for cooperative spectrum sensing in cognitive radio networks," *IEEE J. Sel. Areas Commun.*, vol. 31, no. 11, pp. 2209–2221, Nov. 2013.
[22] E. Basar, M. Wen, R. Mesleh, M. Di Renzo, Y. Xiao, and H. Haas, "Index modulation techniques for next-generation wireless networks," *IEEE Access*, vol. 5, pp. 16693–16746, 2017.
[23] C. Cortes and V. Vapnik, "Support-vector networks," *Mach. Learn.*, vol. 20, pp. 273–297, Oct. 1995.
[24] A. Géron, *Hands-On Machine Learning With Scikit-Learn and Tensor-Flow: Concepts, Tools, and Technologies to Build Intelligent Systems*, 1st ed., N. Tache, Ed. Sebastopol, CA, USA: O'Reilly Media, 2017.[Online]. Available: http://shop.oreilly.com/product/0636920052289.do
[25] R. P. Brent and P. Zimmermann, *Modern Computer Arithmetic*. Cambridge, U.K.: Cambridge Univ. Press, 2010.
[26] H. David and H. Nagaraja, "Basic distribution theory," in *Order Statistics* (Wiley Series in Probability and Statistics). Hoboken, NJ, USA: Wiley, 2003, ch. 2, sec. 2.1, pp. 9–11.
[27] Y. Xiao, S. Wang, L. Dan, X. Lei, P. Yang, and W. Xiang, "OFDM with interleaved subcarrier-index modulation," *IEEE Commun. Lett.*, vol. 18, no. 8, pp. 1447–1450, Aug. 2014.
[28] R. Abu-alhiga and H. Haas, "Subcarrier-index modulation OFDM," in *Proc. IEEE 20th Int. Symp. Pers., Indoor Mobile Radio Commun.*, Tokyo, Sep. 2009, pp. 177–181.

[29] D. Tsonev, S. Sinanovic, and H. Haas, "Enhanced subcarrier index modulation (SIM) OFDM," in *Proc. IEEE GLOBECOM*, Houston, TX, USA, Dec. 2011, pp. 728–732.
[30] T. Mao, Q. Wang, and Z. Wang, "Generalized dual-mode index modulation aided OFDM," *IEEE Commun. Lett.*, vol. 21, no. 4, pp. 761–764, Apr. 2017.
[31] R. Y. Mesleh, H. Haas, S. Sinanovic, C. W. Ahn, and S. Yun, "Spatial modulation," *IEEE Trans. Veh. Technol.*, vol. 57, no. 4, pp. 2228–2241, Jul. 2008.
[32] A. Younis, N. Serafimovski, R. Mesleh, and H. Haas, "Generalised spatial modulation," in *Proc. Conf. Rec. 4th Asilomar Conf. Signals, Syst. Comput.*, Pacific Grove, CA, USA, Nov. 2010, pp. 1498–1502.
[33] S. Lu, I. A. Hemadeh, M. El-Hajjar, and L. Hanzo, "Compressed-sensing-aided space-time frequency index modulation," *IEEE Trans. Veh. Technol.*, vol. 67, no. 7, pp. 6259–6271, Jul. 2018.

JEONGBIN SEO received the B.S. degree from the Department of Electronics Engineering, Pusan National University, Busan, South Korea, in 2019, where he is currently pursuing the Ph.D. degree in electronics engineering. His research interests include the index modulation and applying machine learning in communication systems.

HEETAE JIN received the B.S. degree from the Department of Electronics Engineering, Pusan National University, Busan, South Korea, in 2016, where he is currently pursuing the Ph.D. degree in electronics engineering. His research interests include the V2V and V2X communications and applied machine learning in communications.

DONGHEE YI received the B.S. and M.S. degrees from the Department of Electronics Engineering, Pusan National University, Busan, South Korea, in 2015 and 2017, respectively, where he is currently pursuing the Ph.D. degree in electronics engineering. His research interests include the ultrasonic signal processing and applied machine learning in communications.

SUK CHAN KIM (Senior Member, IEEE) received the B.S.E. degree (summa cum laude) in electronics engineering from Pusan National University (PNU), Busan, South Korea, in February 1993, and the M.S.E. and Ph.D. degrees in electrical engineering from the Korea Advanced Institute of Science and Technology (KAIST), Daejeon, South Korea, in February 1995 and 2000, respectively. He has been a Professor with the Department of Electronics Engineering, PNU, since 2002. His current research interests include mobile communications, statistical signal processing, and applied machine learning for healthcare and communications. He is a member of the Institute of Electronics Engineers of Korea (IEEK) and the Korean Institute of Communication Sciences (KICS). He received the Haedong Paper Award from KICS, in 2005.